Research Article | Vol. 25, No. 9 | 1 May 2017 | OPTICS EXPRESS 10241
Optics EXPRESS

Effective procedure for determination of unknown vibration frequency and phase using time-averaged digital holography

MARIO STIPČEVIĆ,[1,*] NAZIF DEMOLI,[2] HRVOJE SKENDEROVIĆ,[2] MARTIN LONČARIĆ,[1] ANTON RADMAN,[1] JADRANKO GLADIĆ[2] AND DAVORIN LOVRIĆ[2]

[1]*Photonics and Quantum Optics, Center of Excellence for Advanced Materials and Sensing Devices, Ruđer Bošković Institute, Bijenička cesta 54, HR-10000 Zagreb, Croatia*
[2]*Institute of Physics, Bijenička cesta 46, HR-10000 Zagreb, Croatia*
**mario.stipcevic@irb.hr*

Abstract: In time-averaged digital holography (TADH), one records a hologram of a periodically oscillating object by using the exposure time typically much longer than the oscillating period. Problems arise when the total available exposure time is restricted or when the oscillation period is unknown. In this work we investigate effects of short exposure time to the quality of the recorded hologram and show that, to record high fidelity information in a shortest possible time, close estimates of the oscillating period and the phase are required. To that end we propose an advanced procedure based on short hologram exposures that allows obtaining such estimates. The procedure is efficient both in the number of recordings and their total exposure time.

OCIS codes: (090.0090) Holography; (090.1995) Digital holography; (100.2650) Fringe analysis.

References and links

1. R. L. Powell and K. A. Stetson, "Interferometric vibration analysis by wavefront reconstruction," J. Opt. Soc. Am. **55**(12), 1593–1598 (1965).
2. N. Verrier and M. Atlan, "Absolute measurement of small-amplitude vibrations by time-averaged heterodyne holography with a dual local oscillator," Opt. Lett. **38**(5), 739–741 (2013).
3. N. Demoli, J. Mestrović, and I. Sović, "Subtraction digital holography," Appl. Opt. **42**(5), 798–804 (2003).
4. N. Demoli, "Use of optical fiber bundle in digital image plane holography," Opt. Quantum Electron. **45**(8), 861–871 (2013).
5. J. P. Chambard, V. Chalvidan, X. Carniel, and J. C. Pascal, "Pulsed TV – holography recording for vibration analysis applications," Opt. Lasers Eng. **25**, 343–360 (1996).
6. M. Leclercq, M. Karray, V. Isnard, F. Gautier, and P. Picart, "Evaluation of surface acoustic waves on the human skin using quasi-time-averaged digital Fresnel holograms," Appl. Opt. **52**(1), A136–A146 (2013).
7. P. A. A. M. Somers and N. Bhattacharya, "A new method for processing time averaged vibration patterns: linear regression," Strain **52**(4), 264–275 (2016).
8. M. Karray, P. Christophe, M. Gargouri, and P. Picart, "Digital holographic nondestructive testing of laminate composite," Opt. Eng. **55**(9), 095105 (2016).
9. B. P. Thomas, S. A. Pillai, and C. S. Narayanamurthy, "Investigation on vibration excitation of debonded sandwich structures using time-average digital holography," Appl. Opt. **56**(13), F7–F13 (2017).
10. G. O. Rosvold and O. J. Løkberg, "Effect and use of exposure control in vibration analysis using TV holography," Appl. Opt. **32**(5), 684–691 (1993).
11. O. J. Løkberg, "ESPI – The ultimate holographic tool for vibration analysis?" J. Acoust. Soc. Am. **75**, 1783–1791 (1984).
12. W.-C. Wang, C.-H. Hwang, and S.-Y. Lin, "Vibration measurement by the time-averaged electronic speckle pattern interferometry methods," Appl. Opt. **35**(22), 4502–4509 (1996).
13. A. J. Moore, D. P. Hand, J. S. Barton, and J. D. C. Jones, "Transient deformation measurement with electronic speckle pattern interferometry and a high-speed camera," Appl. Opt. **38**(7), 1159–1162 (1999).
14. M. Yamamoto, H. Yamamoto, and Y. Hayasaki, "Photon-counting digital holography under ultraweak illumination," Opt. Lett. **34**(7), 1081–1083 (2009).
15. N. Demoli, H. Skenderović, and M. Stipčević, "Digital holography at light levels below noise using a photon-counting approach," Opt. Lett. **39**(17), 5010–5013 (2014).
16. N. Demoli, H. Skenderović, and M. Stipčević, "Time-averaged photon-counting digital holography," Opt. Lett. **40**(18), 4245–4248 (2015).

#287427 https://doi.org/10.1364/OE.25.010241
Journal © 2017 Received 24 Feb 2017; revised 8 Apr 2017; accepted 13 Apr 2017; published 25 Apr 2017

17. A. D. Wilson, "Characteristic functions for time-average holography," J. Opt. Soc. Am. **60**(8), 1068–1071 (1970).
18. M. Abramowitz and I. Stegun, *Handbook of Mathematical Functions with Formulas, Graphs, and Mathematical Tables*, NIST, 1972, p. 360.
19. J. M. Gere and S. P. Timoshenko, *Mechanics of Materials*, PWS Publishing Company, 1997.
20. D. Lovrić, Z. Vucić, J. Gladić, N. Demoli, S. Mitrović, and M. Milas, "Refined Fourier-transform method of analysis of full two-dimensional digitized interferograms," Appl. Opt. **42**(8), 1477–1484 (2003).
21. J. Gladić, Z. Vučić, and D. Lovrić, "Reducing phase retrieval errors in Fourier analysis of 2-dimensional digital model interferograms," Opt. Lasers Eng. **45**(8), 868–876 (2007).

1. Introduction

Time-averaged digital holography (TADH) is a powerful technique for detecting resonant vibrations of objects. By applying the TADH, surface harmonic vibrations are converted into the Bessel interference fringes [1]. However, the Bessel description of fringe information is accurate under the restriction of having the hologram exposure time τ either equal to or much greater than the period of vibration T. Such a definition of τ is sufficient for most of the TADH applications. In recent applications, the TADH has been combined with heterodyne detection of optical modulation side bands to attain absolute measurement of small-amplitude vibrations [2]. Fast and good-quality confocal imaging of distant objects via an optical fiber bundle has been demonstrated by combining subtraction holography method [3] and direct accessing to image acquisition interface buffers in which the time-averaged holograms have been temporarily stored [4]. Retrieving the vibration amplitude and phase (necessary for some applications, see Ref [5].) has been demonstrated by recording the quasi-time-averaged holograms to visualize and analyze acoustic waves propagating at the surface of the human skin [6]. Linear regression method has been used for processing vibration patterns yielding the vibration amplitude as an argument of true Bessel function, not its absolute value, thus offering the noise level reduction [7]. The structural health monitoring of machine related components is important for maintenance strategies [8]. The TADH technique has been successfully applied in structural mechanics problems such as vibration analysis of laminated composite glass-epoxy [8] or detection of defects in sandwich structures [9]. In this very recent study [9], the honeycomb sandwich panels have been inspected through square wave excitation approach thus yielding fast identification of defects.

However, in cases that require identifying the precise value of resonant frequency, one has to investigate the sensitivity of τ with respect to T when $\tau \neq nT$. How different is the recorded fringe pattern for $\tau < T$ from the one that accurately describes vibration at $\tau = T$? Or, when can we assume that τ is long enough to satisfy the condition $\tau \gg T$? Moreover, in practical applications with unknown vibration frequency neither of the exposure conditions is automatically satisfied. Typically, the problem of recording holograms with exposures shorter than the vibration period occurs in TV holography, where the standard video system (25 or 30 frames per second) has a fixed exposure time which limits its use regarding the fidelity of measured fringe patterns in lower frequency range. By combining the readout shutter setting and integration mode of the CCD camera, the effective τ can be controlled and correct fringe patterns obtained from $\tau \sim 0.6T$ upwards [10]. Electronic speckle pattern interferometry (ESPI) is well suited measuring technique to study vibrations [11]. The fringe contrast and measurement sensitivity in time-averaged ESPI has been investigated for the case $\tau = \delta + NT$, where δ is the time difference between the vibration period and the shutter opening time and N is the number of cycles. The introduced mismatch errors have been found to be proportional to δ and inversely proportional to the vibration frequency [12]. The use of a high speed camera in the ESPI has allowed measuring both the harmonic vibrations and the transient deformations. For very short exposures ($\tau \ll T$), the integral describing recorded hologram has been approximated by a linear expansion, simplifying the analysis [13]. Photon-counting approach, useful in recording digital holograms under harsh experimental conditions of a very weak signal [14, 15], has also been used for recording time-averaged digital

Optics EXPRESS

holograms [16]. In that study, first the fringe function comprising the main parameters affecting the hologram recording has been defined and then the conditions for satisfactory hologram reconstructions investigated. Many randomized short exposures have been applied instead of long ones to fulfill the TADH conditions in general [16]. Although many studies in the TADH have quantified vibrations, studies on the precise limits of the parameter τ in order to achieve high fidelity of the fringe function are still lacking, as well as the procedure for detecting and identifying unknown vibration frequency.

In this paper, we propose a procedure for determining the frequency and the phase of an unknown harmonic vibration. To accomplish this task, we investigate the fidelity of the fringe information in relation to the exposure time of the recorded holograms. First, we use the correlation measures to calibrate the phase synchronization of the system, and then, we find the minimum number of holograms required to record the complete information on the measured vibration.

2. Preliminaries

2.1 Characteristic fringe function

Consider an off-axis image plane digital holography setup with a sinusoidally vibrating object. The object is, for example, set to vibration by a nearby loudspeaker driven by an electronic signal generator. The driving force $F(t)$ exerted on the object is characterized by amplitude V and frequency f_0, i.e. $F(t) = V\sin(2\pi f_0 t)$ where $T = 1/f_0$ is the vibration period. For simplicity, we treat in this study only one dimensional vibration of the object, since the generalization to more dimensions is straightforward. The momentary displacement of the surface of the oscillating object can be described by

$$z(x,t) = h(x)\sin\left[2\pi f_0 (t - t_d)\right], \tag{1}$$

where x denotes spatial coordinate, t_d is time delay between the phases of the generated sine signal and oscillating surface, and the surface amplitude $h(x)$ depends on the excited vibration mode(s) and driving force. In our study, the constant t_d will be precisely determined for the time synchronization purpose. The interference of two light beams, namely the reference and object, at the detector plane can be described by

$$I(x,t) = a(x) + b(x)cos\left[\varphi_r(x) - \varphi_s(x,t)\right], \tag{2}$$

where $a(x)$ is the background intensity, $b(x)$ is modulation amplitude, $\varphi_r(x) = (2\pi/\lambda)x\sin(\vartheta)$ is the phase of the static reference beam, $\varphi_s(x,t) = -(4\pi/\lambda)z(x,t)$ the phase of the object beam, λ is wavelength, and ϑ is the inclination angle of the reference beam. The hologram exposure is defined by $E(x) = \int_0^\tau I(x,t)\,dt$, where $E(x)$ is the exposure time. Characteristic fringe function (CFF) that describes concomitant fringes [17] of a surface vibrating with a period T is given by:

$$M_\tau(x) = \frac{1}{\tau}\int_{t_0}^{t_0+\tau} \exp\left[i\Phi(x)\sin\frac{2\pi}{T}(t - t_d)\right]\mathrm{d}t \tag{3}$$

where τ is recording time of the hologram (exposure), $\Phi(x)=(4\pi/\lambda)h(x)$ is the phase value of the object beam at the position *x*, and $0\le t_0<T$. The observable (namely the hologram) recorded by the camera is absolute value of CFF, i.e. $|M_\tau(x)|$.

In a general case, the recording time (exposure) can be written as $\tau=NT+\Delta T$, where N is the number of full cycles ($N=0,1,2,...$) and ΔT is a duration of the last incomplete cycle of recording ($0\le\Delta T<T$). Furthermore, the recording may start at an arbitrary time delay t_0. Thus, for a general CFF we can write:

$$M_\tau(x)=\frac{NT}{\tau}J_0\left[\Phi(x)\right]+\frac{1}{\tau}\int_{t_0}^{t_0+\Delta T}\exp\left[i\Phi(x)\sin\frac{2\pi}{T}t\right]\mathrm{d}t. \tag{4}$$

Apparently, the complete hologram corresponds to Bessel function of the first kind ($|M_\tau(x)|=J_0\left[\Phi(x)\right]$) and is obtained for exposure times equal to the integer number of periods $(\tau=NT)$ or for an infinitely long exposure $(\tau\to\infty)$. However, the complete information can be also achieved from the half-period of vibration. Equation (4) can be expressed as follows,

$$\begin{aligned}M_\tau(x)&=\frac{1}{\tau}\int_{\frac{T}{4}}^{\frac{3T}{4}}\exp\left[i\Phi(x)\sin\frac{2\pi}{T}t\right]\mathrm{d}t=\frac{1}{\pi}\int_{\frac{\pi}{4}}^{\frac{3\pi}{4}}\exp\left[i\Phi(x)\sin\theta\right]\mathrm{d}\theta\\&=\frac{1}{\pi}\int_{-\pi/4}^{\pi/4}\exp\left[i\Phi(x)\cos\theta\right]\mathrm{d}\theta=J_0\left[\Phi(x)\right]\end{aligned} \tag{5}$$

where we have substituted $\theta=(2\pi/T)\,t$, and in the last step we have used well-known integral representation of J_0 [18]. This shows that, indeed, a full reconstruction can be obtained by the half-period exposure.

2.2 Displacement of a cantilever beam

In this work, we use a cantilever of uniform linear density fixed at one end and driven in the lowest oscillation mode, as shown in Fig. 1. In that mode, the phase corresponding to the displacement of the surface at a distance *x* from the fixed point is described by [19]:

$$\Phi(x)=A_0\left[3\left(\frac{x}{L}\right)^2-2\left(\frac{x}{L}\right)^3+\frac{1}{2}\left(\frac{x}{L}\right)^4\right] \tag{6}$$

where L is the length of the beam and the dimensionless amplitude A_0 is estimated heuristically in a way that the number of fringes in Eq. (3) corresponds to the number of fringes observed in the range $x\epsilon[0,L]$. In our case we have used $A_0=12.9$, which leads to about 5 fringes.

Optics EXPRESS

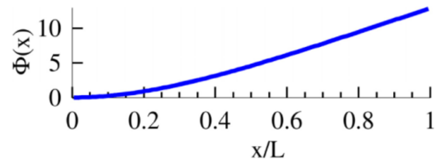

Fig. 1. Displacement $h(x)$ (arbitrary units) of a uniform linear density cantilever beam of length L fixed at $x = 0$, in its lowest oscillation mode.

2.3 Hologram recordings – snapshots

We will generally record a hologram by making a number of short recordings that we name "snapshots", as illustrated in Fig. 2. The snapshots are then averaged by software to obtain the final hologram. Each snapshot has its starting time t_i and exposure τ_i, where $i = 0,1,2,\ldots$ is the index of a snapshot. In case when several snapshots follow each other without a delay, such as in Fig. 2 for snapshots $0-2$, the recorded hologram corresponds to a single exposure whose duration is from the beginning of the first snapshot till the end of the last one. This method of recording is built-in in our setup described below.

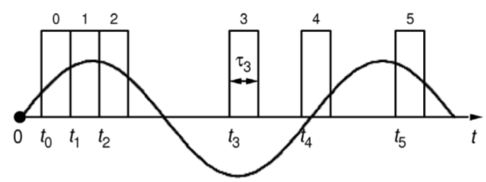

Fig. 2. Illustration of snapshots with respect to the vibration amplitude (sinusoid) of the object.

3. Experimental setup and software

Schematic diagram of our experimental setup for recording holograms is shown in Fig. 3a. For recording holograms we used image plane configuration (imaging lens denoted by L1). The continuous near-Gaussian laser beam from the He-Ne laser (Research Electro-Optics, Model No. 32734, power 2.5 mW, wavelength 633 nm) is split into object and reference beams (collimated by Col1 and Col2) that interfere in front of the digital camera (Basler acA2040-120um) generating an image plane hologram picked up directly by the camera chip (without a lens). The separation angle between the object and reference beams was approximatelly 2 degrees. The camera is equipped with Sony IMX252LLR-C high-speed progressive scan monochrome CMOS sensor having resolution of 2048×1536 pixels, each having size of 3.45×3.45 µm. It features 63% quantum efficiency at 633 nm, has a 12 bit analog-to-digital converter, and a shutter with minimal exposure time of 21 µs.

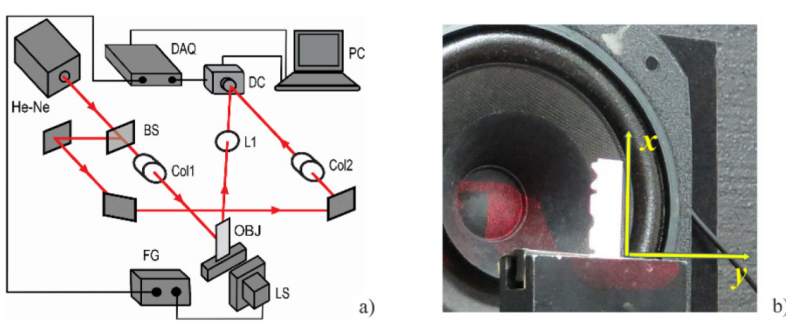

Fig. 3. a) Schematics of the test setup, b) Photography of the object (OBJ) and the loudspeaker (LS).

Optics EXPRESS

The object OBJ is a cantilever made of high strength and high elasticity steel strip cut out from a razor blade (Wilkinson Sword) firmly held at one end while the other one is free. The cantilever is 10 mm wide and has a length of $L \approx 28$ mm. The length is carefully chosen in order to have the lowest vibration mode at $f_0 = 100$ Hz. This has been kept fixed throughout the whole study. The vibration is driven by the loudspeaker (LS) positioned at a distance of 10 cm, as shown in Fig. 3b. The function generator FG (Rigol DG4162) runs in the free mode generating a sinusoidal and a quadratic signal that are in a fixed mutual phase relationship. The sinusoidal signal (amplitude 0.06 V) drives the loudspeaker, while the quadratic signal is sent to the data acquisition board DAQ (National Instruments USB-6259) where it is read by the steering program (written in LabView) running at the personal computer (PC). After a calibration procedure described in Sect. 4, the software becomes aware of the object's vibration phase and can trigger the digital camera (DC) at a precisely known moment within the oscillation period. The phase delay between the loudspeaker and camera trigger can be set with the resolution of 1 μs by programming the FG. This enables us to record holograms with an arbitrary delay with respect to the object's stationary position and with an arbitrary duration, which are essential requirements for this work.

Holograms recorded by the camera are reconstructed using fast Fourier transforms (FFT). One example of the reconstructed hologram of the vibrating cantilever made by a very long exposure ($\tau \gg T$) is shown in Fig. 4a). We extract pixel intensities from the rectangular region of interest shown in Fig. 4b), and average values of pixels with the same x coordinate to obtain a vector of intensities (profile vector) along the x direction, as shown in Fig. 4c), by means of a home-made computer program. The region of interest is 244 pixels long, thus the obtained intensity profile vector has 244 values (components).

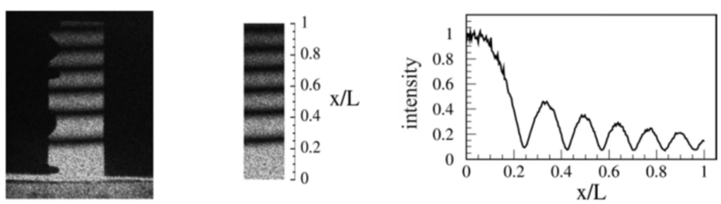

a) b) c)

Fig. 4. a) Reconstructed hologram. b) Region of interest within the reconstructed hologram. c) One-dimensional vector of intensities along x axis obtained by averaging pixels with the same x coordinate in the region of interest.

4. Effects of finite exposure time

As already mentioned in the Introduction, in recording TAHs it is commonly assumed that the recording time τ is much greater than the period of vibration T, since in that case the CFF given by Eq. (3) asymptotically tends to the zeroth order Bessel function of the first kind [16], which may be considered as a “complete” hologram. In this section we study both numerically and experimentally the effects of a finite exposure, notably the exposure shorter than one period, and we investigate the possibility to obtain a (near-) complete hologram by means of a short exposure.

As a measure of similarity of two reconstructed holograms, each represented by its respective intensity profile vectors $\boldsymbol{u}$ and $\boldsymbol{v}$, as explained in the previous section and Fig. 4, we use the normalized cross-correlation of the two vectors:

$$a_{\mathrm{uv}}(k) = \frac{\sum_{i=1}^{N-k}\left(u_i - \bar{u}\right)\left(v_{i+k} - \bar{v}\right)}{\sqrt{\left(\sum_{i=1}^{N-k}\left(u_i - \bar{u}\right)^2\right)\left(\sum_{i=1}^{N-k}\left(v_i - \bar{u}\right)^2\right)}}, \tag{7}$$

where $a_{\mathrm{uv}}(k)$ is the cross-correlation coefficient with a lag k, while u_i and v_i are components of vectors $\boldsymbol{u}$ and $\boldsymbol{v}$ respectively. In this study we are only interested in similarity of aligned holograms, i.e. $a_{\mathrm{uv}}(0)$. Value of the normalized cross-correlation is bound between 1 (identical holograms) and -1 (inverted holograms). In both extreme cases the two holograms are completely determined by each other while for statistically independent holograms the cross-correlation is equal to zero. We therefore define "deviation" of holograms from each other as:

$$D = 1 - \left| a_{\mathrm{uv}}(0) \right|. \tag{8}$$

The deviation D can take on a value between 0 (totally correlated holograms) and 1 (uncorrelated holograms).

4.1 Vibration phase calibration

Before we start our investigation, we must calibrate the system's phase, i.e. determine the overall time delay t_d between the camera trigger and the equilibrium position of the object's surface. This delay is then subtracted by our steering program such that the trigger time $t = 0$ corresponds to the equilibrium node of the sinusoidal vibration of the object. To determine t_d, we first record ten consecutive 1 ms snapshots, as shown in Fig. 2, that span the whole vibration period ($T = 10$ ms) and extract their profile vectors, $\boldsymbol{u}_i, i = 0 \ldots 9$. Then, using Eq. (3) we calculate corresponding theoretical profile vectors $\boldsymbol{v}_i(t_d)$ using an initial value $t_d = 0$, and calculate the total cross-correlation between measured and calculated profile vectors:

$$\mathrm{Corr}(t_d) = \frac{1}{10} \sum_{i=0}^{9} a_{u_i, v_i(t_d)}(0). \tag{9}$$

We repeat the second step of our calculations for a series of 400 values of t_d chosen equidistantly in the range $[0, T]$ (step size thus being 25 µs) and each time we evaluate Eq. (9). There will be a single maximum of total cross-correlation and it will correspond to the condition $t_0 = t_d$. In our case we have obtained $t_d = 4.424$ ms. After this calibration procedure the system's overall delay becomes zero ($t_d = 0$).

To check the calibration visually, we record 10 snapshots, 1 ms exposure each, spanning one whole period, with the first exposition starting at the oscillation node ($t_0 = 0$). Reconstructions and extracted profile vectors and shown in Fig. 5, while Fig. 6 shows theoretical profiles obtained by numerical evaluation of Eq. (3). Due to inevitable noise in the recording device (camera) and the speckle noise, the experimental intensity profiles do not feature the maximum visibility and therefore do not reach zero, as opposed to the numerical evaluation which neglects noise. The cross-correlation between the experimental and theoretical intensity profiles is sensitive to the difference in their shape and relative displacement along x-axis. Nevertheless, we note a good alignment between the experimental and theoretical profiles shown in Fig. 5 and Fig. 6. One may see that in the snapshots made at moments of the fastest cantilever movement (1st, 5th, 6th and 10th) there is a clearly visible fringe, while for the two snapshots made around the slow moving regions of sinusoid hill (3rd) and valley (8th) the snapshots resemble a still photo of the object. The central symmetry of the first half and the last half of the series of snapshots, as well as the symmetry between two halves, follow from the corresponding symmetries of the sinusoid.

Optics EXPRESS

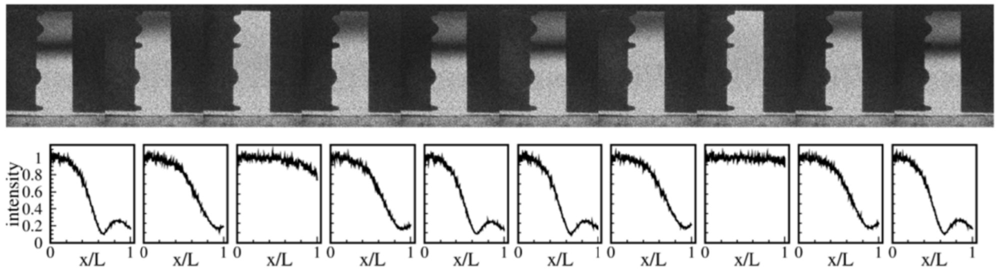

Fig. 5. Reconstructions of 10 consecutive holographic snapshots, each made with exposure time of 1 ms (up). Intensity profiles extracted from snapshots (down).

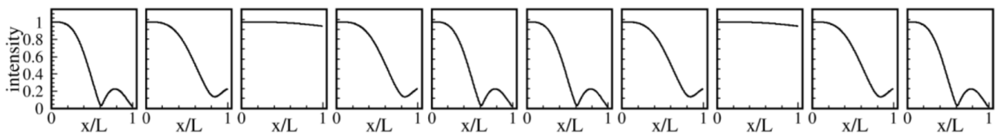

Fig. 6. Numerical calculations of intensity profiles corresponding to measurements in Fig. 5.

As a more precise check of calibration, we repeat the calibration procedure now expecting to get $t_d \approx 0$. To that end, we calculate the total cross-correlation $\mathrm{Corr}(t_0)$ for a series of times around $t_0 = 0$ in steps of 25 µs. Plot of the obtained curve shown in Fig. 7 confirms a good alignment. In order to estimate the precision of this method, we record 10 series of snapshots and repeat the procedure. The obtained average peak position is –3 µs with the root-mean-square error of 17 µs, which is about $T/588$. To appreciate this precision, it is interesting to note that it takes about 290 µs for the sound wave to travel 10 cm from the loudspeaker to the object and that this delay varies by 0.5 µs/K with air temperature.

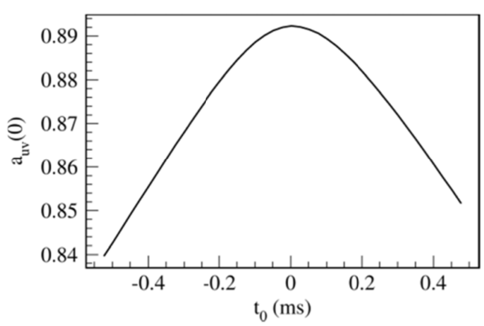

Fig. 7. Total cross-correlation between ten consecutive reconstructed holograms (each recorded with a 1 ms exposure and shown in Fig. 5) and corresponding theoretical predictions shifted in time by t_0.

Apparently, the precision with which the overall delay t_d can be determined by this method depends on, and is limited by, several factors, notably: signal-to-noise ratio in the intensity profiles of the reconstructed holograms, the number of snapshots, air temperature variations, jitter between the trigger pulse and actual exposure of the camera, etc.

4.2 Hologram quality as a function of exposure and its phase

To investigate the influence of the incomplete cycle described by the second term in Eq. (4), we record 20 consecutive snapshots of 1 ms exposure each and reconstruct averaged holograms of cumulative exposure durations from 1 to 20 ms, as shown in Fig. 8 in the upper two rows. As expected, we obtain a complete hologram for the full period (10 ms exposure). This effect is more clearly seen in the corresponding intensity profiles drawn in the middle two rows, and confirmed with theoretically calculated profiles in the bottom two rows.

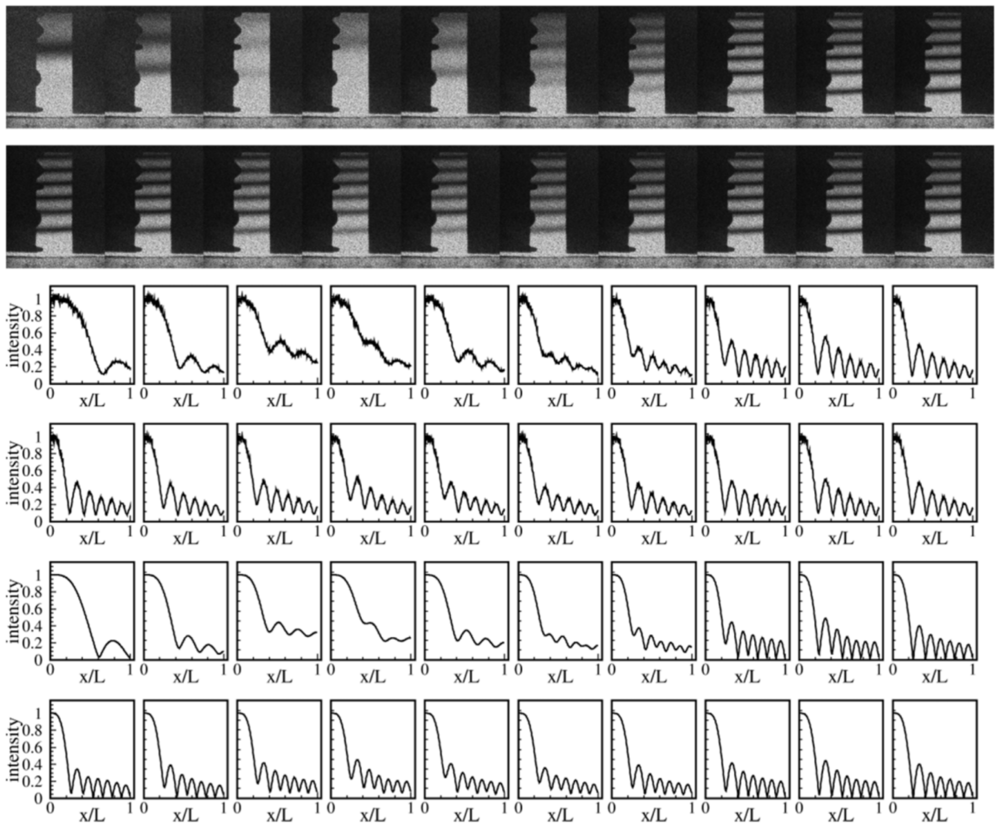

Fig. 8. Reconstructed holograms (upper two rows), their intensity profiles (middle two rows) and simulations (bottom two rows) for exposures lasting 1, 2, 3, ..., 20 ms, starting at the oscillation node ($t_0 = 0$).

More generally, Fig. 9 shows calculated deviation curves for exposures starting at different delays t_0 and lasting up to 5 full periods. The deviation rises quickly when the exposure is not equal to a multiple of the period, but stays below the certain envelope for any t_0. Interestingly, this result does not depend on the delay t_0 of the exposure with respect to the surface equilibrium position. This can be understood by noting that recording over a full period, regardless of when the recording has begun, contains complete information about the vibration of the object and therefore it must be sufficient to define a complete hologram. On the contrary, for finite exposures, when $\Delta T \neq 0$, the resulting hologram deviates from the complete one, and the deviation depends on t_0.

Optics EXPRESS

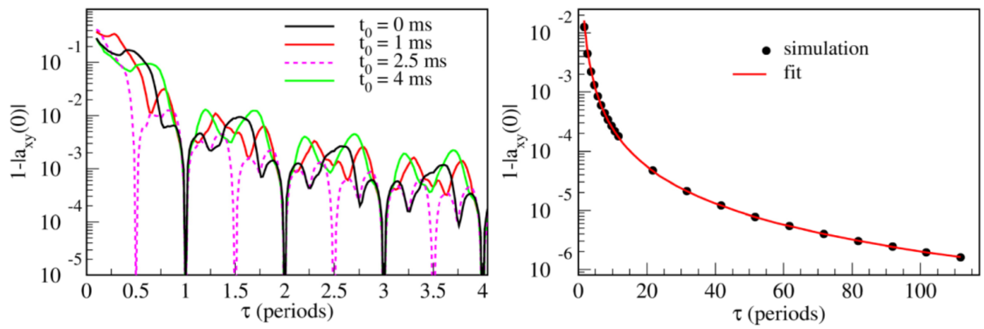

Fig. 9. Deviation of the reconstructed time-averaged hologram from the reconstructed complete hologram, as a function of exposure time τ expressed in vibration periods $T = 10$ ms. Several deviation functions for different starting times of the exposure within the period overlap (left). Maximum deviation as a function of the exposure time (right).

In order to estimate the maximum deviation as a function of the exposure time we have calculated numerically the maximum deviation in each period and fitted a smooth function through these points, as shown in Fig. 9 b). Numerically, the fitted function asymptotically converges to $1/\tau^2$ for large exposure times τ :

$$D(t) = \frac{0.02}{(\tau/T)^2}\left(1+\frac{2.3}{\tau/T}\right). \tag{10}$$

4.3 The shortest exposure time required for recording a complete hologram

In Fig. 9 one can readily note that, for this special case of sinusoidal oscillation, it is possible to obtain the complete hologram from a recording that lasts only one half of the period. This is achieved provided the recording is made between two stationary points of the object's movement, i.e. between the top and the bottom of the sinusoidal movement of the object's surface. Namely, in that case the other half of the period consists of repeating of exactly the same movement path but in the time reversed order, thus contributing no new information to the hologram.

To verify experimentally that the full information can be obtained from the half-period exposure, we have recorded a hologram by averaging five successive exposures of 1 ms starting at 2.5 ms after the sinusoidal node (equilibrium), as shown in Fig. 10.

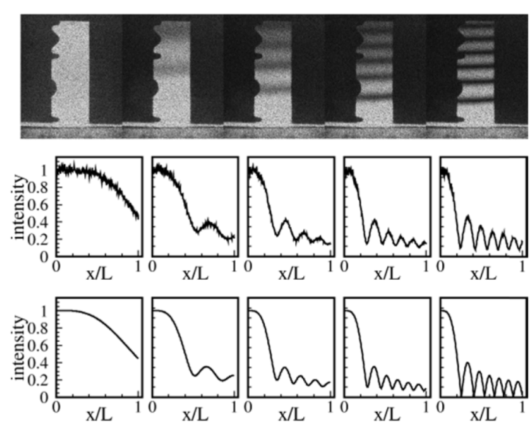

Fig. 10. Reconstructed holograms for exposures of duration of 1,2,3,4, and 5 ms starting 2.5 ms after the equilibrium (top)s, extracted intensity profiles (middle), and calculated intensity profiles (bottom).

Optics EXPRESS

From this example we learn that it is possible to record a complete hologram in a time shorter that the object's oscillation period in cases when all information on the vibration is contained within a part of the period, such as in the case of pure sinusoidal vibration. However, this is not generally the case and then recording lasting one whole period is both necessary and sufficient.

5. Determination of unknown vibration period and phase

So far we have investigated methods of recording a complete TADH in the shortest possible time. The method which makes use of exposure over an integer number of periods requires knowing the vibration period with a high precision, while even faster half-period exposure method requires knowing both the period and the phase of vibration. However, in case of an unknown or inaccessible object, both period and phase are generally unknown.

In this section we develop an algorithm for determining both frequency and phase of a periodically vibrating object by recording and analyzing only a few holographic snapshots. We assume that a broad interval $[T_{\min}, \ T_{\max}]$, in which the unknown vibration period T lies, can be robustly estimated via a general observation (size and shape of the object, expected vibration mode, etc.), and that the snapshots can be made with an exposure time significantly shorter than the oscillating period (i.e. quasi-stationary).

We analyze the object vibration by laser digital interferometry, i.e. by recording and analyzing the two dimensional interference patterns (fringes) created by reflection of laser beam from the object. If the object vibrates harmonically, the interference fringes locally change their phase according to the sinusoidal law,

$$\psi(t) = a + b\sin(\omega t + \varphi), \tag{11}$$

where $\psi(t)$ is the phase of a fringe at an arbitrary point in the hologram at time t, $\omega = 2\pi / T$ is the circular frequency of the phase change, while a, b and φ are free parameters (a and b describing the background noise). In calculations of $\psi(t)$ we have used our already developed programs providing the sub-pixel accuracy in determination of the position of the interference maxima in inverse Fourier space [20, 21]. In order to minimize the effects of noise, we have calculated the phase differences between subsequent snapshots, and retrieved the particular phases $\psi(t)$ from these differences. Figure 11 shows fringe phases of our object vibrating at $T = 10$ ms extracted from series of 100 snapshots, taken every 0.1 ms, and recorded with exposure times of: 0.1 ms, 0.4 ms and 1.0 ms.

We note that at short enough exposure time τ snapshots are quasi-stationary, which results in sharp fringes whose phase is well determined, as may be seen in Visualization 1 for $\tau = 0.1$ ms and Visualization 2 for $\tau = 0.4$. Each Visualization consists of 100 consecutive snapshots of the vibration induced interference patterns (in xy plane, as defined in Fig. 3b), each depicted by its time stamp. On the other hand, at a longer exposure time of $\tau = 1$ ms snapshots are not quasi-stationary anymore and fringes appear blurred when the object is moving fast and are sharp only near the stationary points Visualization 3. This results in larger noise and dispersion of measured phases around the sinusoidal behavior. However, short exposure times may increase shot noise. This can be remedied in two ways. One is to enlarge the intensity of the light source and the other to switch to the hologram recording via photon counting. Using this technique we have demonstrated good hologram recording at signal levels as low as two orders of magnitude below the shot noise via homodyne detection [15].

Optics EXPRESS

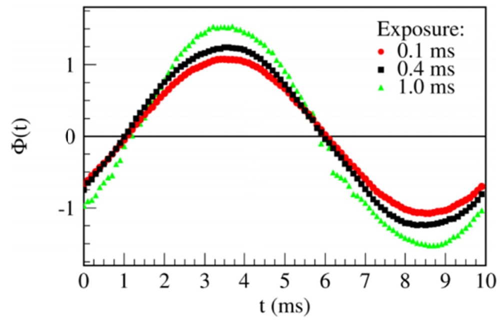

Fig. 11. Measured fringe phases of 100 consecutive snapshots, taken every 0.1 ms, of the steel cantilever vibrating with period $T = 10$ ms. Three series of phases are shown for different snapshot exposure times: 0.1 ms, 0.4 ms and 1 ms. Temporal development of fringe phases for the three exposure times is shown in Visualization 1, Visualization 2, and Visualization 3, respectively.

Our procedure for determination of the vibration period and phase is optimized for the smallest required number of snapshots. It is divided into two stages: rough and fine estimation of both the vibration period and phase.

In the first stage, one takes the first snapshot at an arbitrary moment t_0, followed by a series of further snapshots taken at times $t_0 + \alpha^{j-1} T_{\min}$, where $j = 0,1,2,\ldots$, and determines fringe phase difference $\Delta\varphi_j$ between j-th snapshot and the snapshot taken at t_0, using the above described method. The method works best for $2 \le \alpha \le 10$. If the starting times of two snapshots are too close, the phase difference will not be discernible from zero due to the experimental noise. However, for the smallest j for which $\Delta\varphi_j$ can be clearly determined, one stops and calculates the rough estimate of the period as $T_R = \left(2\pi / \Delta\varphi_j\right) \alpha^{j-1} T_{\min}$. This method is very efficient since the maximum number of snapshots required is equal to $1 + \log_\alpha \left(T_{\max} / T_{\min}\right)$.

In the second stage, one takes N sequential snapshots at time instants $t_i = t_0 + i\left(T_R / N\right)$, and determines $\psi(t_i)$ as fringe phase differences between i-th snapshot and snapshot taken at time t_0. Finally, the points $\left(t_i, \psi(t_i)\right)$ are subject to the fitting procedure described below. In order to solve the system of N equations analytically, we bring it to the form of the system of linear equations:

$$\psi(t) = A + B \sin\left(\frac{2\pi}{T} t\right) + C \cos\left(\frac{2\pi}{T} t\right) \tag{12}$$

where now A, B, C and T are the four unknown parameters that may be determined by the least-squares fit of the function Eq. (12) to $N \ge 4$ measured points. The overall data set variance is given by:

$$R^2 = \sum_{i=0}^{N-1} \left(A + B \sin\left(\omega t_i\right) + C \cos\left(\omega t_i\right) - \psi\left(t_i\right) \right)^2. \tag{13}$$

Minimizing this quantity with respect to A, B and C leads to the linear system of equations:

Optics EXPRESS

$$\begin{bmatrix} N & \sum \sin(\omega t_i) & \sum \cos(\omega t_i) \\ \sum \sin(\omega t_i) & \sum (\sin(\omega t_i))^2 & \sum \sin(\omega t_i)\cos(\omega t_i) \\ \sum \cos(\omega t_i) & \sum \sin(\omega t_i)\cos(\omega t_i) & \sum (\cos(\omega t_i))^2 \end{bmatrix} \times \begin{bmatrix} A \\ B \\ C \end{bmatrix} = \begin{bmatrix} \sum \psi(t_i) \\ \sum \psi(t_i)\sin(\omega t_i) \\ \sum \psi(t_i)\cos(\omega t_i) \end{bmatrix} \tag{14}$$

which may be solved by Cramer rule or Gaussian elimination method. However, T is still unknown in Eq. (14). We have noted heuristically that it is sufficient to scan T from $T_{\max}$ down to $T_{\min}$ in relatively coarse steps of 2 percent (or smaller) and search for the first sharp minimum that appears or, alternatively, the smallest value of R^2, as a function of T in the given interval. Once this coarse minimum is found, Newton's method can be applied to refine the search for the true minimum value of R^2 and thus the corresponding period estimate T_E at which the minimum occurs. Computer-simulated examples plots of R^2 for $N = 4, 5, 7$ and 10 points, with vibration period chosen to be $T = 10$ ms, are shown in the left panel of Fig. 12. Four points is an absolute minimum required to solve Eq. (14), but using more points makes search for a global minimum more robust against experimental errors of phases $\psi(t_i)$.

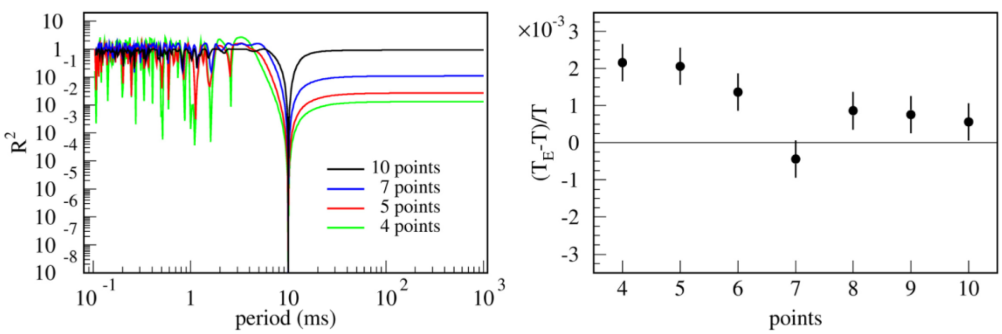

Fig. 12. Simulations of the overall variance R^2 for an object periodically vibrating with the period of 10 ms. Simulations for $N = 4,5,7$ and 10 points chosen uniformly within the period are drawn in different colors (left). Relative error of the period T_E estimated by our method using N measured phases obtained from snapshots of the cantilever vibrating with period $T = 10$ ms (right).

Solving the system in Eq. (14) for T_E simultaneously yields best estimates for parameters A, B and C. The phase of the object's vibration phase φ defined in Eq. (11), with respect to the time moment t_0, is given by:

$$\cos(\varphi) = \frac{B}{\sqrt{B^2 + C^2}}; \sin(\varphi) = \frac{C}{\sqrt{B^2 + C^2}}. \tag{15}$$

To test the procedure, we used it to estimate vibration period of our cantilever oscillating at $T = 10$ ms by making snapshots with exposure of 0.4 ms. We used the search interval [0.1, 1000] ms. Right panel of Fig. 12 shows relative error of the period estimate T_E obtained for $N = 4 - 10$ points. In our case, already with 4 points the relative error $(T_E - T)/T$ of 2×10^{-3} is not far from the uncertainty set by the measurement noise.

6. Conclusions

To record accurate information by the TADH the hologram exposure time is one of the most critical parameters and should equals multiple of the vibration period. The errors appearing for non-integer values of the exposure time are analyzed by numerical simulations and experimental measurements. We have found that exact hologram can be obtained with the exposure time equal to one half of the vibration period, provided that the phase information of the vibration is known. Therefore, we have developed an efficient procedure for determining both the frequency and the phase of an unknown harmonic vibration. The procedure is based on two estimation stages, namely rough and fine, where in the rough stage one determines the time interval between hologram snapshots while in the fine stage one estimates the vibration period. The proposed procedure has proven effective in both the number of recorded holographic snapshots and the total exposure time, for which we believe it can be exploited in various practical applications (especially those in biomedical and industrial applications, as indicated in Sec. 1).

Funding

Croatian Science Foundation (IP-2014-09-7515), Croatian Ministry of Science Education and Sports (533-19-14-0009).